Check for updates

Tracking electron motion driving the Suzuki–Miyaura cross-coupling reaction

Noriyuki Takai,[a] Takuro Tsutsumi, [iD][b] Tetsuya Taketsugu [iD][bc] and Takao Tsuneda [iD] *[cd]

The electron motion driving the transmetalation process of the Suzuki–Miyaura cross-coupling reaction is elucidated based on the reactive orbital energy theory (ROET). We investigated the transmetalation process in the palladium-catalyzed synthesis of biphenyl from phenylboronic acid and chlorobenzene, focusing on two proposed pathways: the boronate mechanism and the oxo-palladium mechanism. Intrinsic reaction coordinate (IRC) calculations were performed for both mechanisms, followed by ROET analysis. The results indicate that the boronate mechanism proceeds with a lower activation barrier and a simpler reaction pathway, while also exhibiting electron motion patterns consistent with experimental observations. Furthermore, the ROET analysis clarified the electronic roles of the organoboronic acid and the ancillary ligand in a manner consistent with experimental findings. These results demonstrate that ROET provides a novel perspective on metal-catalyzed reactions by offering insights into the underlying electron motions.

1. Introduction

Cross-coupling reactions form C–C or C-heteroatom bonds between an organic electrophile and an organometallic nucleophile, mediated by a transition metal catalyst.[1,2] These reactions are among the most widely employed in the synthesis of pharmaceuticals and functional organic materials due to their high selectivity and yield, and their compatibility with a wide range of functional groups. Cross-coupling reactions are generally understood to proceed *via* a three-step catalytic cycle. Taking the reaction of an organic halide electrophile (R–X) and an organometallic nucleophile (R′–M) catalyzed by a Pd complex bearing ancillary ligands (L) as an example, the mechanism is considered to proceed as follows:

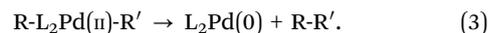1. Oxidative addition: the Pd(0) complex reacts with the electrophile to form a Pd(II) complex:

$$L_2Pd(0) + R\text{-}X \rightarrow R\text{-}L_2Pd(\text{II})\text{-}X, \quad (1)$$

2. Transmetalation: the organometallic nucleophile donates its organic moiety to the Pd complex:

$$R\text{-}L_2Pd(\text{II})\text{-}X + R'\text{-}M \rightarrow R\text{-}L_2Pd(\text{II})\text{-}R' + M\text{-}X, \quad (2)$$

and

3. Reductive elimination: the two organic ligands bound to Pd couple to form the final product:

$$R\text{-}L_2Pd(\text{II})\text{-}R' \rightarrow L_2Pd(0) + R\text{-}R'. \quad (3)$$

Several variations of cross-coupling reactions have been proposed, which differ primarily in the nature of the organometallic nucleophile. Major examples include the Kumada–Tamao–Corriu,[3,4] Suzuki–Miyaura,[5] Negishi,[6] Stille,[7] and Hiyama[8] reactions. The key mechanistic distinction among these reactions lies in the transmetalation step, during which the organic group is transferred from the nucleophile to the transition metal center, as illustrated in eqn (2). The efficiency and applicability of each cross-coupling variant are largely governed by the mechanism of transmetalation, which depends on the type of nucleophile employed. This step has been investigated extensively through theoretical approaches, such as reaction energy profiling and calculation of activation barriers.[9] However, practical utility is often determined less by reactivity and more by selectivity and yield, particularly the ability to form desired bonds without by-products. To address this aspect, it is necessary to elucidate the electronic roles of the nucleophile, transition metal, and ancillary ligands. Conventional electronic analyses of metal-catalyzed reactions have primarily relied on orbital-based approaches, such as bonding orbital analysis,[10,11] as well as localized orbital methods, including natural bond orbital (NBO) analysis[12] and intrinsic bond orbital (IBO) analysis.[13] However, these types of orbital analyses are inherently limited in their ability to comprehensively elucidate the full picture of

[a] *Graduate School of Chemical Sciences and Engineering, Hokkaido University, Sapporo 060-8628, Japan*

[b] *Department of Chemistry, Faculty of Science, Hokkaido University, Sapporo 060-0810, Japan*
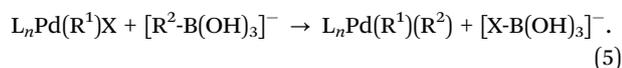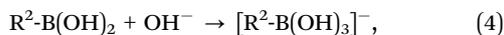
[c] *Institute for Chemical Reaction Design and Discovery (WPI-ICReDD), Hokkaido University, Sapporo 001-0021, Japan*

[d] *Graduate School of Science Technology and Innovation, Kobe University, Nada-ku, Kobe, Hyogo 657-8501, Japan. E-mail: takaotsuneda@sci.hokudai.ac.jp*

This journal is © the Owner Societies 2025

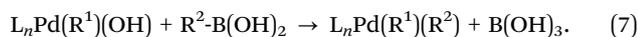*Phys. Chem. Chem. Phys.*, 2025, **27**, 17261–17269 | **17261**

catalytic reactions where nucleophiles, transition metals, and ancillary ligands are intricately involved.

The Suzuki–Miyaura reaction is a cross-coupling between an organoboron compound and an organohalide catalyzed by a palladium complex.[1,9,14] It is one of the most widely used cross-coupling methodologies[15] and has become indispensable in the synthesis of pharmaceuticals, functional materials, and agrochemicals. Organoboron reagents used in this reaction are notable for environmentally friendly nature, mild reaction conditions, and high tolerance to functional groups. It is well established that the presence of a base is essential for the reaction to proceed efficiently.[16] Although its reactivity is lower than that of the Kumada reaction, which uses Grignard reagents, the Suzuki–Miyaura reaction offers several advantages: it proceeds under milder conditions and is tolerant of moisture and air, and minimizes by product formation when properly optimized. Two primary mechanisms have been proposed for the transmetalation step of the Suzuki–Miyaura reaction, depending on the manner in which the organoboron species interacts with the base:[17]

1. Boronate mechanism:[18–20] the base reacts with the boronic acid to generate an anionic boronate species, which then participates in transmetalation:

$$R^2\text{-B(OH)}_2 + OH^- \rightarrow [R^2\text{-B(OH)}_3]^-, \qquad (4)$$

$$L_n\text{Pd}(R^1)X + [R^2\text{-B(OH)}_3]^- \rightarrow L_n\text{Pd}(R^1)(R^2) + [X\text{-B(OH)}_3]^-. \qquad (5)$$

2. Oxo-palladium mechanism:[21] the Pd(II) complex first reacts with the base to form a Pd–OH species, which subsequently reacts with the boronic acid:

$$L_n\text{Pd}(R^1)X + OH^- \rightarrow L_n\text{Pd}(R^1)(OH) + X^-, \qquad (6)$$

$$L_n\text{Pd}(R^1)(OH) + R^2\text{-B(OH)}_2 \rightarrow L_n\text{Pd}(R^1)(R^2) + \text{B(OH)}_3. \qquad (7)$$

Experimental studies using isolated Pd complexes – either halide-type (L_n Pd(R^1)X) or hydroxo-type (L_n Pd(R^1)(OH)) – have shown that the hydroxo species reacts significantly faster, suggesting that the oxo-palladium mechanism may be dominant.[22] In contrast, recent theoretical studies have reported lower activation barriers for the boronate mechanism, concluding that it is more favorable thermodynamically.[21] Notably, even the boronate pathway includes Pd–OH formation steps that are not rate-limiting, and thus both views may be reconciled. However, relying solely on reaction barriers is insufficient to explain the preference for the boronate mechanism. A deeper understanding requires a detailed electronic structure analysis to uncover the underlying driving forces that selectively promote the boronate pathway. Until recently, the absence of electronic analytical methods capable of comprehensively elucidating the driving forces of metal-catalyzed reactions has hindered research of this kind.

Reactive orbital energy theory (ROET)[23] is an electronic theory that elucidates the electron motions driving chemical reactions based on quantitative changes in orbital energies.[24] ROET is founded on a statistical mechanical theorem stating that the direction of maximum energy change during a reaction corresponds to the direction in which the orbital energies of the electron-transfer orbitals, which are called reactive orbitals, undergo the most significant variation.[23,25] It has also been demonstrated that the electrostatic force exerted on nuclei by reactive orbitals during a reaction corresponds to the negative gradient of their orbital energies.[26] Therefore, the driving force of electrons in a reaction can be qualitatively discussed in terms of the magnitude of the orbital energy gradient. Furthermore, a one-to-one correspondence between reaction pathways and reactive orbitals has been established.[27] ROET-based reaction analysis (ROET analysis) enables comprehensive and quantitative electronic-theoretical analyses of diverse reactions. When ROET was applied to representative organic redox reactions, it was found that the initial direction of electron transfer closely aligned with the direction of electron flow depicted by curly arrows in traditional organic reaction mechanisms.[28] Recently, we performed a ROET analysis of the Kumada cross-coupling reaction, where a Pd complex acts as the catalyst, chlorobenzene as the organic halide electrophile, and a Grignard reagent as the organometallic nucleophile. The analysis revealed the electron motion mechanisms that drive each step of this metal-catalyzed reaction and clarified the respective roles of the Pd complex and the Grignard reagent. In the transmetalation process, it was shown that electron donation from the Pd complex – supported by the ancillary ligand – and electron acceptance by the Grignard reagent *via* the MgCl site together facilitate the electron flow. This enabled the identification of the electronic roles of the Pd complex, the organometallic nucleophile, and the organic electrophile.

In this study, we apply ROET analysis to the Suzuki–Miyaura cross-coupling reaction. By comparing the results with those of the Kumada reaction, we aim to elucidate – based on electron motion – the reason behind the superior performance of organoboronic acids used as nucleophiles in the Suzuki–Miyaura reaction. Furthermore, we investigate two proposed transmetalation mechanisms – the boronate mechanism and the oxo-palladium mechanism-through ROET analysis to determine, from an electronic perspective, which pathway is more favorable. Lastly, by integrating the results of previously analyzed oxidative addition and reductive elimination processes, we analyze the overall electron motion driving the entire catalytic cycle and evaluate its consistency with experimental findings. This approach aims to provide guiding principles for the future design of novel cross-coupling reactions.

2. Computational details

The transmetalation step in the Suzuki–Miyaura cross-coupling reaction is investigated for the two possible mechanisms: the boronate mechanism and the oxo-palladium mechanism. To enable comparison with the ROET analysis of the Kumada cross-coupling reaction, we examined the same biphenyl-forming reaction as used in our previous study.[29] In the transmetalation process, the palladium complex coordinated
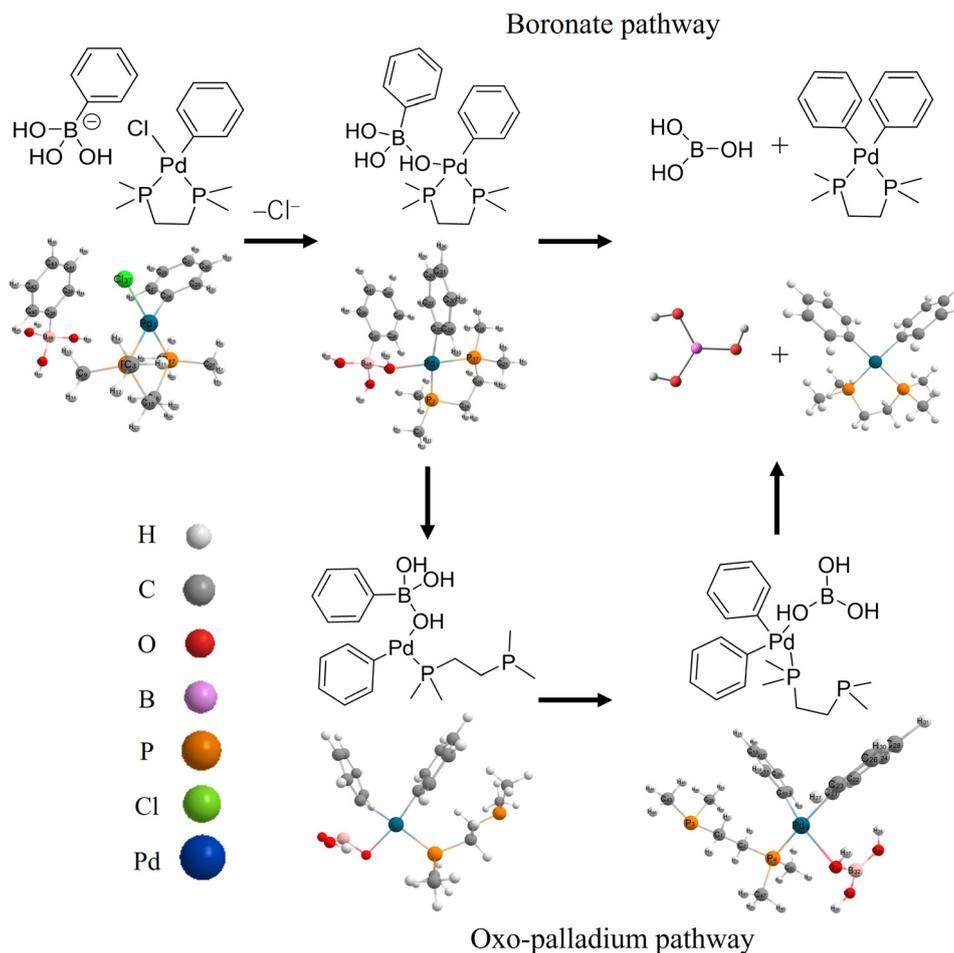
Fig. 1 Two possible mechanisms for the transmetalation step in the Suzuki–Miyaura cross-coupling reaction – the boronate mechanism and the oxo-palladium mechanism – along with their corresponding computational models and optimized intermediate structures. Geometry optimizations were carried out at the ωB97XD/LanL2DZ (Pd) and cc-pVDZ (for all other atoms) level of theory. The computational models of the intermediates for the two mechanisms were constructed with reference to the previous calculations by Ortuno *et al.*[21]

with two phenyl groups, Ph–Pd(II)dmpe-Ph, where 1,2-bis(dimethylphosphino)ethane (dmpe) serves as the ancillary ligand, is generated from the phenylboronate anion (Ph–B(OH)$_3$$^-$) and the palladium complex Ph–Pd(II)dmpe-Cl, which is coordinated with one phenyl group and one chloro group. The oxidative addition process, in which Ph–Pd(II)dmpe-Cl is formed from the Pd(0) complex Pd(0)dmpe and chlorobenzene (Ph–Cl), and the reductive elimination process, in which biphenyl (Ph–Ph) and a Pd complex are produced from Ph–Pd(II)dmpe-Ph, have already been calculated and verified in a previous study.[29] Therefore, these processes will not be examined in the present study. Fig. 1 shows the two proposed mechanisms for the transmetalation process in the Suzuki–Miyaura reaction, along with the computational models used to evaluate them and the optimized geometries of key intermediates.

Intrinsic reaction coordinate (IRC) calculations were carried out using the reaction models described above. Transition state (TS) structures were located using the single-component (SC) and double-sphere (DS) artificial force induced reaction (AFIR) methods.[30] The AFIR method applies artificial forces to steer the system along plausible reaction pathways, making it particularly suitable for identifying transition states in complex systems, such as metal-catalyzed reactions, where multiple transition states often lie in close proximity. All SC-AFIR and DS-AFIR calculations were performed using a development version of GRRM23 program.[31] Details of the AFIR calculations corresponding to each IRC path are summarized in Scheme S1. Only key points are highlighted below. To obtain the quantitative orbital energies required for the ROET analysis, all calculations employed Kohn–Sham density functional theory (DFT) using ωB97XD functional, which includes long-range correction for exchange functionals[32] and dispersion interactions.[33] This is because reactions involving metal complexes usually entail long-range charge transfer governed by long-range exchange interactions, and their large, flexible structures are affected by long-range dispersion forces. Indeed, benchmark calculations on the MOBH35 set have shown that functionals incorporating both long-range correction and dispersion effects yield the most accurate reaction barriers for metal-containing systems.[34] For TS and IRC calculations, the LanL2DZ basis set[35]

This journal is © the Owner Societies 2025

Phys. Chem. Chem. Phys., 2025, **27**, 17261–17269 | **17263**

was used for Pd, and cc-pVDZ[36] for all other atoms. This combination was chosen to maximize accuracy within the constraints of computational resources for TS modeling. For the initial AFIR search, a less demanding basis set was adopted: def2-SV(P) for Pd, Cl, and Mg atoms, and STO-3G for all others. Solvent effects were modeled using the conductor-like polarizable continuum model (CPCM) with diethyl ether as the solvent. In the two-step transmetalation process, where explicit solvent participation is essential, two diethyl ether molecules were explicitly included in the computational model. All DFT calculations were carried out using the Gaussian 16 program.[37] The Cartesian coordinates of all optimized structures, including the reactants, intermediates, and products, are provided in Table S1.

ROET analysis was performed based on the molecular structures and orbital energies obtained along the intrinsic reaction coordinate (IRC) pathway.[23] By plotting orbital energies at each point along the IRC and tracking their evolution, we analyzed the orbital energy changes associated with the reaction. In our orbital energy-tracking program, the MO that exhibits the maximum overlap between successive points is automatically identified using the following procedure:

1. First, the molecular orbital coefficient matrix $\mathbf{C}$ is normalized and orthogonalized using the overlap integral matrix $\mathbf{S}$,

$$\mathbf{C}' = \mathbf{S}^{1/2}\mathbf{C}. \tag{8}$$

2. Next, at each step k along the IRC, the inner product matrix $\mathbf{O}$ between the normalized and orthogonalized molecular orbital coefficient matrix $\mathbf{C}'$ and that of the previous step $k - 1$ is calculated,

$$\mathbf{O}_{k,k-1} = \mathbf{C}'_k \mathbf{C}'^{\dagger}_{k-1}. \tag{9}$$

3. Then, the orbital energy changes are traced by connecting the orbitals with the maximum inner product values.

4. Finally, the pair of the most stabilized occupied orbital and the most destabilized virtual orbital in a reaction process are identified as the occupied and unoccupied reactive orbitals (OROs and UROs).

The ROET diagram is constructed using the OROs identified at each point along the IRC. In transition-metal-catalyzed reactions, multiple electron transfer events often occur within a single reaction process. To capture this, we divided the analysis into early, middle, and late stages, allowing for a more detailed tracking of electron motion that drives the reaction. It should be noted that the boundaries between these stages vary depending on the specific reaction and do not necessarily correspond to distinctive features on the IRC (such as TS). Although changes in electron distribution correspond to the evolution of OROs, it is often difficult to intuitively identify electron transfers solely from canonical orbital representations. To address this, we also provide diagrams analogous to curly arrows commonly used in organic reaction mechanisms. These arrows were manually drawn based on visual inspection of changes in electron distribution across multiple reaction stages. While this process could potentially be automated in future implementations, it was performed manually in the present study.

To further clarify the evolution of OROs, we also created animations showing their continuous change along the reaction coordinate. These animations are provided as SI MP4 files. For further details on the ROET method, readers are referred to previous studies.[27,38]

3. Results and discussion

Let us analyze the transmetalation process of the Suzuki–Miyaura cross-coupling reaction using ROET analysis, based on the IRCs calculated for the two proposed mechanisms introduced above: the boronate mechanism and the oxo-palladium mechanism. This analysis provides insight into the relative favorability of each pathway by examining the underlying electron motions. Particular emphasis is placed on the electronic roles of the boronic acid and the ancillary ligand in each mechanism.

3.1. Boronate mechanism of the transmetalation reaction

TS and IRC calculations were first carried out for the boronate mechanism in eqn (4) and (5). The results indicate that this mechanism proceeds through two distinct steps. Fig. 2(a) presents the potential energy curve along the IRC corresponding to the first step of the boronate mechanism. As illustrated in the schematic molecular structures in the figure, the first step of the boronate mechanism involves the coordination of a hydroxyl group from the boronate anion to the Pd center of the palladium complex. The intermediate formed in this step, as revealed by our calculations, corresponds to the oxo-palladium intermediate previously proposed in experimental studies.[22] This result indicates that the boronate mechanism is not in conflict with experimental observations. According to the potential energy profile, the activation barrier for this step is 15.69 kcal mol^{-1}, and the reaction is mildly exothermic, with a reaction energy of 2.34 kcal mol^{-1}. These values indicate that the process is thermodynamically and kinetically feasible under ambient conditions. In the previous study,[21] the activation barrier for the first step of the boronate mechanism is slightly higher, at 18.9 kcal mol^{-1}, whereas the reaction is endothermic with a reaction energy of −10.8 kcal mol^{-1}. In contrast, the present results indicate that this step proceeds more readily than previously suggested. As shown in Fig. 2(b), the occupied reactive orbital involved in this process is identified as HOMO−12 of the reactant. Although the electron density associated with this orbital changes significantly throughout the reaction, the corresponding electron motion is illustrated with curly arrows in Fig. 2(a) for clarity. These arrows indicate that the initial stage of the reaction is driven by electron transfer from the ancillary ligand to the Pd center and then to the hydroxyl group of the boronate anion. In the later stage, the electron flow continues from the Pd center through the hydroxyl group to the phenyl moiety of the boronate anion. Notably, although the overall electron flow of the reaction is expected to proceed from the boronate anion to the chloro group, this transfer is not observed in the reactive

17264 | *Phys. Chem. Chem. Phys.*, 2025, **27**, 17261–17269

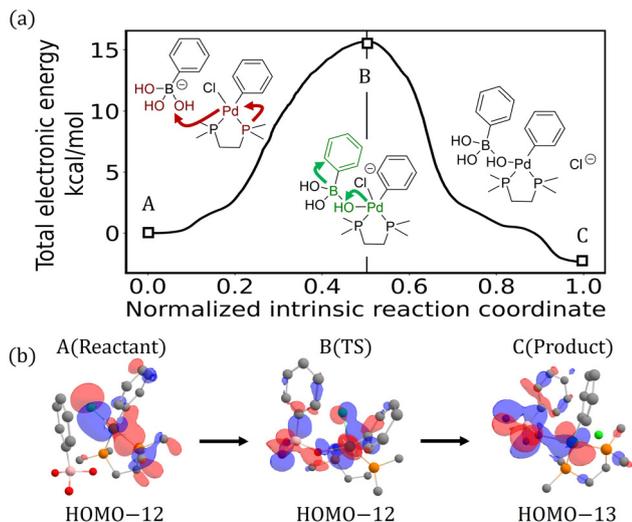This journal is © the Owner Societies 2025

Fig. 2 Potential energy profile along the intrinsic reaction coordinate for the first-step transmetalation process in the boronate mechanism of the Suzuki–Miyaura cross-coupling reaction, accompanied by (a) the electron motion driving the reaction as revealed by ROET analysis and (b) the corresponding changes in electron distribution of the identified reactive orbitals. In this step, an oxo-palladium intermediate is formed via the reaction between the phenylboronate anion (Ph–B(OH)$_3^-$) and a Pd complex bearing 1,2-bis(dimethylphosphino)ethane as the ancillary ligand. Red–brown arrows indicate electron transfer in the early stage of the reaction, while green arrows represent electron transfer in the late stage. The functional groups that play an active role in driving the electron motion at each reaction stage are highlighted in the corresponding colors. For a more detailed depiction of electron motions, refer to the attached animations.
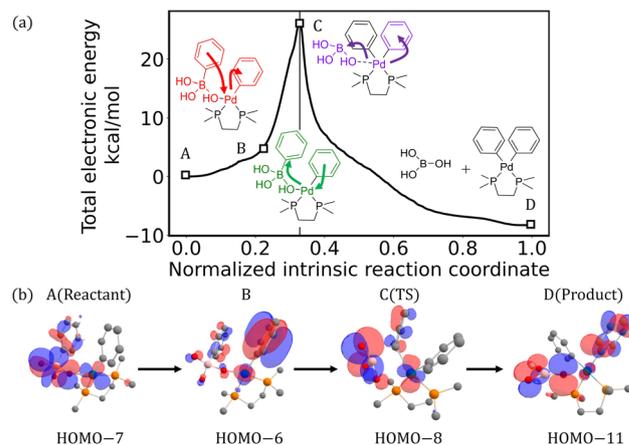

Fig. 3 Potential energy profile along the intrinsic reaction coordinate for the second-step transmetalation process in the boronate mechanism of the Suzuki–Miyaura cross-coupling reaction, accompanied by (a) the electron motion driving the reaction as revealed by ROET analysis, and (b) the corresponding changes in electron distribution of the identified reactive orbitals. In this step, the phenyl group from the boronic acid is transferred to the Pd center of the oxo-palladium intermediate, while the remaining B(OH)$_3$ moiety dissociates, resulting in the formation of Ph–Pd(II)(dmpe)-Ph. Red–brown arrows indicate electron transfer in the early stage of the reaction, green arrows represent the middle stage, and purple arrows correspond to the late stage. The functional groups that play an active role in driving the electron motion at each reaction stage are highlighted in the corresponding colors. For a more detailed depiction of electron motions, refer to the attached animations.

orbital motion. This finding suggests that the electron transfer to the chloro group does not directly drive the reaction, but rather contributes indirectly by enhancing the electron-donating character of the Pd center.

Fig. 3(a) presents the potential energy curve along the calculated IRC for the second step of the boronate mechanism. The figure shows that the activation barrier for this process is 26.52 kcal mol^{-1}, and the reaction is exothermic with a reaction energy of 8.31 kcal mol^{-1}. This step is also expected to proceed under ambient conditions, although it is the rate-determining step within this mechanism. In the previous study,[21] the activation energy is reported as 32.6 kcal mol^{-1}, and the reaction energy as 13.2 kcal mol^{-1}. Compared to those values, the present result supports the feasibility of this step at room temperature. On the other hand, the orbital energy profile for this process shown in Fig. S3(a) reveals only minor changes in the energy of the ORO throughout the reaction. This result indicates that electron motion plays a relatively limited role in driving this step of the reaction. Fig. 3(b) illustrates the evolution of the ORO, identified as HOMO−7 of the reactant, along the IRC. A distinguishing feature of this orbital is the significant electron transfer occurring between the phenyl groups during the reaction. The corresponding electron motion, depicted with curly arrows, is shown in the molecular structure in Fig. 3(a). As indicated by the curly arrows, the early stage of the reaction is driven by electron transfer between the phenyl

groups. In the later stage, electron motion is directed toward the dissociating boric acid (B(OH)$_3$), together with the phenyl group that was coordinated to the Pd center. These results suggest that the reaction proceeds via electron transfer between the phenyl groups, mediated by the Pd center and the boric acid moiety. As a result, the phenyl group of phenylboronic acid (PhB(OH)$_3$) becomes coordinated to the Pd center, and electrons are ultimately donated to the B(OH)$_3$ fragment, promoting its dissociation. The role of electron transfer from the Pd center to the B(OH)$_3$ fragment in driving this process is further supported by the orbital energy profile shown in Fig. S3(b). In this profile, the corresponding electron transfer occurs near the TS and is accompanied by a substantial decrease in orbital energy, which in turn generates an electrostatic force that guides the nuclei along the reaction coordinate.

3.2. Oxo-palladium process of the transmetalation reaction

Next, we examine the oxo-palladium mechanism, an alternative transmetalation pathway for the Suzuki–Miyaura reaction, as depicted in eqn (6) and (7). This mechanism originates from the oxo-palladium intermediate formed during the first step of the boronate mechanism.[21]

Fig. 4(a) shows the potential energy curve along the IRC calculated for the first step of the oxo-palladium mechanism. Unlike the previous study using monodentate ancillary ligands,[21] the present analysis yields a reaction pathway that more closely reflects the actual process in which a bidentate ancillary ligand becomes monodentate during the course of the
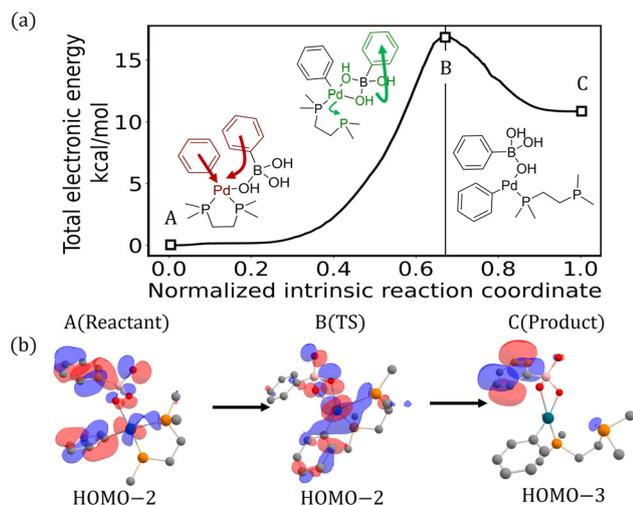
This journal is © the Owner Societies 2025

Phys. Chem. Chem. Phys., 2025, **27**, 17261–17269 | **17265**

Fig. 4 Potential energy profile along the intrinsic reaction coordinate for the first-step transmetalation process in the oxo-palladium mechanism of the Suzuki–Miyaura cross-coupling reaction, accompanied by (a) the electron motion driving the reaction as revealed by ROET analysis, and (b) the corresponding changes in electron distribution of the identified reactive orbitals. In this process, one arm of the bidentate ligand, 1,2-bis(dimethylphosphino)ethane, dissociates from the oxo-palladium intermediate formed in the first step of the boronate mechanism. Red–brown arrows indicate early-stage electron transfer, while green arrows represent the late-stage electron transfer. The functional groups that play an active role in driving the electron motion at each reaction stage are highlighted in the corresponding colors. For a more detailed depiction of electron motions, refer to the attached animations.

Fig. 5 Potential energy profile along the intrinsic reaction coordinate for the second-step transmetalation process in the oxo-palladium mechanism of the Suzuki–Miyaura cross-coupling reaction, accompanied by (a) the electron motion driving the reaction as revealed by ROET analysis, and (b) the corresponding changes in electron distribution of the identified reactive orbitals. In this process, the phenyl group of the phenylboronic acid coordinates to the Pd center. Red–brown arrows indicate electron transfer in the early stage, green arrows represent the middle stage, and purple arrows correspond to the late stage. The functional groups that play an active role in driving the electron motion at each reaction stage are highlighted in the corresponding colors. For a more detailed depiction of electron motions, refer to the attached animations.

reaction. As shown in the figure, this process has an activation barrier of 16.95 kcal mol^{-1} and is exothermic, with a reaction energy of −10.86 kcal mol^{-1}. This indicates that the reaction proceeds slightly more easily than in the previous study, which reported an activation energy of 18.6 kcal mol^{-1} and a reaction energy of −13.0 kcal mol^{-1}. However, since the reaction is still endothermic, the thermal favorability of this process remains limited. The changes in the ORO, identified as HOMO−2 of the reactant and illustrated in Fig. 4(b), indicate that electrons are initially transferred from the phenyl group to the Pd center of the Pd complex, and subsequently accumulate on the phenyl group of the phenylboronic acid. To aid interpretation, the electron motion throughout the reaction is depicted using curly arrows in Fig. 4(a). While the overall direction of electron transfer is consistent with this schematic, in the middle to late stages of the reaction, electron motion associated with the dissociation of the Pd–P bond is also observed. This electronic behavior is reflected in the corresponding structural changes of the complex. As shown in Fig. S4(a), the reaction is driven by electron transfer to the phenylboronic acid moiety near the transition state. However, the ORO energy variation is relatively small, indicating that this electron motion does not serve as the primary driving force for the overall reaction.

Next, the potential energy curve along the IRC calculated for the second step of the oxo-palladium mechanism is shown in Fig. 5(a). The second step involves a reaction in which the ancillary ligand becomes monodentate, followed by coordination
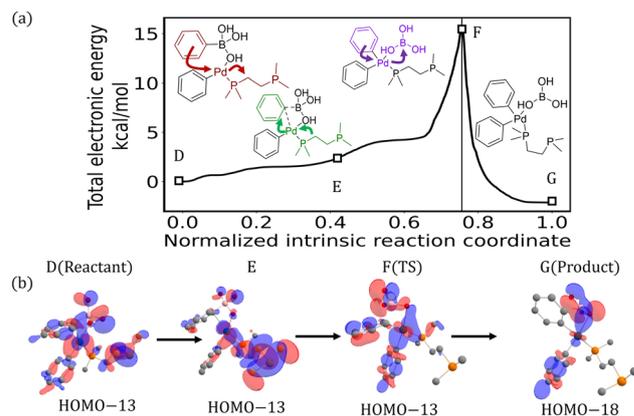
of the phenyl group from the phenylboronic acid to the Pd center. As shown in the figure, this process has an activation barrier of 15.75 kcal mol^{-1} and is exothermic, with a reaction energy of 2.14 kcal mol^{-1}. This result is nearly identical to that reported in a previous study,[21] which estimated the activation energy and reaction energy to be 15.1 kcal mol^{-1} and 2.2 kcal mol^{-1}, respectively. Note, however, that the structure of the ancillary ligand differs substantially. These values suggest that the reaction can proceed under ambient conditions. Fig. 5(b) displays the evolution of the ORO, identified as HOMO−13 of the reactant, during this step. The figure reveals that the initially delocalized electron distribution becomes localized on the boronic acid and the phenyl group originally coordinated to the Pd center as the reaction progresses. To visualize the electron flow driving each stage of the reaction, the corresponding curly arrow diagram is provided in Fig. 5(a). According to the diagram, in the early stage of the reaction, electrons move from the phenyl group of the phenylboronic acid to the ancillary ligand *via* the Pd center. In the middle stage, the direction of electron flow reverses, enabling coordination of the phenyl group to the Pd center. Finally, in the late stage, electrons transfer from the phenyl group, through the Pd center, to the boronic acid moiety. As shown in the orbital energy profile in Fig. S4(b), the key driving force of this reaction process is the electron transfer that occurs in the intermediate stage, from the phenyl group of the phenylboronic acid to the ancillary ligand *via* the Pd center. This electron motion facilitates the coordination of the phenyl group to the Pd center.

For the third step of the oxo-palladium mechanism, the potential energy curve along the IRC calculated is presented in Fig. 6(a). As shown in the figure, this step has an activation barrier of 35.30 kcal mol^{-1} and is exothermic, with a reaction

17266 | *Phys. Chem. Chem. Phys.*, 2025, **27**, 17261–17269

This journal is © the Owner Societies 2025

energy of about 21.48 kcal mol^{-1}. The activation energy obtained here is slightly higher than the 32.6 kcal mol^{-1} reported in the previous study,[21] while the reaction energy is considerably more positive than the previously reported value of 13.2 kcal mol^{-1}. This discrepancy likely arises from the fact that the prior study treated this step as part of the boronate pathway without accounting for the re-coordination of the ancillary ligand to its bidentate form, which is explicitly considered in the present analysis. While the reaction is expected to proceed at room temperature, the relatively high barrier suggests that it would occur slowly. However, due to the substantial exothermicity, the reaction is considered thermodynamically favorable. Fig. 6(b) shows the evolution of the ORO, identified as HOMO−8 of the reactant. The change in electron distribution suggests that electrons are transferred from the newly coordinated phenyl group to the ancillary ligand, facilitating the reformation of the Pd–P coordination bond. This electron motion is illustrated with curly arrows in Fig. 6(a). In the early stage of the reaction, electrons flow from the newly coordinated phenyl group to the Pd center. Subsequently, in the middle stage, the electron flow continues toward the ancillary ligand, promoting the reformation of the Pd–P bond. In the late stage, the direction of electron flow reverses. According to the orbital energy profile shown in Fig. S4(c), the ORO energy variation proceeds gradually after the transition state. This slow progression contributes to the high activation barrier observed for this step. Therefore, the electron motion does not strongly drive the reaction, which likely accounts for the sluggishness of the oxo-palladium mechanism overall.

Fig. 6 Potential energy profile along the intrinsic reaction coordinate for the third-step transmetalation process in the oxo-palladium mechanism of the Suzuki–Miyaura cross-coupling reaction, accompanied by (a) the electron motion driving the reaction as revealed by ROET analysis, and (b) the corresponding changes in electron distribution of the identified reactive orbitals. In this process, the ancillary ligand returns to its bidentate coordination, and the boronic acid that was coordinated to the Pd center dissociates. Red–brown arrows indicate electron transfer in the early stage of the reaction, green arrows represent the middle stage, and purple arrows correspond to the late stage. The functional groups that play an active role in driving the electron motion at each reaction stage are highlighted in the corresponding colors. For a more detailed depiction of electron motions, refer to the attached animations.

3.3. Mechanism of Suzuki–Miyaura cross-coupling reaction

Finally, based on the above results, we summarize the overall picture of the electron motion that drives the Suzuki–Miyaura cross-coupling reaction, as revealed by the ROET analysis. Fig. 7 presents an overview of the electron motion across the three main processes of the Suzuki–Miyaura reaction. The ROET analysis results for the oxidative addition and reductive elimination processes were established in our previous study.[29] Including these two steps in the analysis reveals that the ancillary ligand plays only a supportive role at the very beginning of the transmetalation process. Experimental studies have shown that the ancillary ligand is involved exclusively in the oxidative addition and reductive elimination processes,[15] and the present ROET findings support this interpretation. Furthermore, the ancillary ligand is typically chosen for its strong electron-donating ability, and this characteristic is reflected in the electron motion that drives the reaction. It is worth noting that the oxo-palladium mechanism, which is not the focus of this mechanism, involves the dissociation and reassociation of the ancillary ligand's coordination bonds. Thus, participation of the ancillary ligand in that pathway is unavoidable. From an experimental perspective, this supports the view that the boronate mechanism is the more likely operative pathway under standard Suzuki–Miyaura conditions. In contrast, the boronic acid moiety plays a more active role: together with the Pd center, it serves as a conduit for electron transfer between the two phenyl groups. After initially donating electrons to the chloro group on the Pd complex, it continues to accept electrons throughout the reaction, until it eventually dissociates. Surprisingly, the electron transfer to the chloro group does not directly drive the transmetalation process; rather, it exerts an indirect effect by making the Pd complex more electron-rich. This observation highlights a limitation of conventional electron-pushing formalism, which typically interprets such electron transfers as direct driving forces behind the reaction – a perspective that fails to capture the subtleties revealed by ROET analysis.

Let us compare the reaction mechanism of the Suzuki–Miyaura reaction with that of the Kumada reaction. In terms of activation barriers, the highest barrier in the Kumada reaction is 7.6 kcal mol^{-1} (in the second step), whereas in the Suzuki–Miyaura reaction it reached 26.5 kcal mol^{-1} for the boronate mechanism (second step) and 35.3 kcal mol^{-1} for the oxo-palladium mechanism (third step). This substantial difference indicates that the transmetalation step is not rate-determining in the Kumada reaction, while it becomes the rate-determining step in the Suzuki–Miyaura reaction. In the Kumada reaction, the reductive elimination step is the rate-determining one. Comparing the electron motion that drives the reaction, the Kumada reaction proceeds through a complex sequence of electron transfers, starting with an initial electron transfer to the Grignard reagent. In contrast, in the boronate mechanism of the Suzuki–Miyaura reaction, the reaction proceeds *via* direct electron exchange between functional groups that are actively involved in the reaction. Taken together, these findings suggest that the low susceptibility of the Suzuki–Miyaura
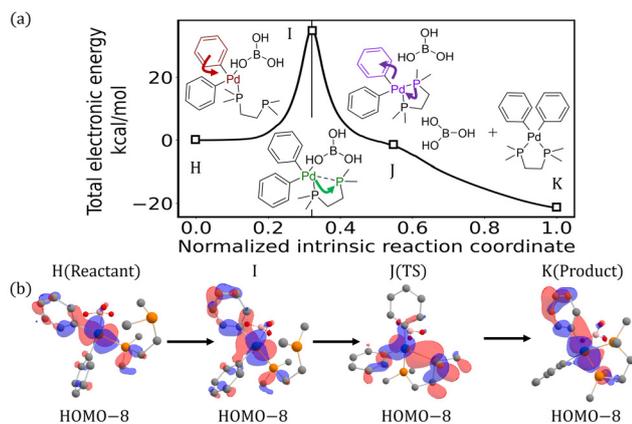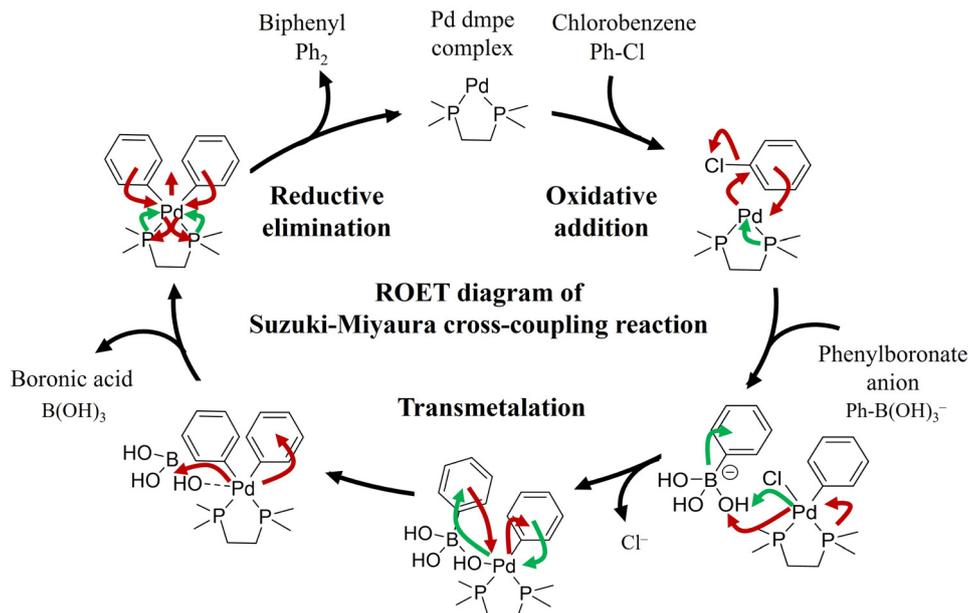
This journal is © the Owner Societies 2025

Phys. Chem. Chem. Phys., 2025, **27**, 17261–17269 | **17267**

Fig. 7 Whole mechanism of Suzuki–Miyaura cross-coupling reaction based on ROET and potential energy analyses. The oxidative addition and reductive elimination processes were analyzed in our previous study using ROET, and the results were reported in ref. 29. The red–brown and green arrows indicate the electron motions at the early and late stages, respectively, for each process.

reaction to side reactions stems from the fact that the transmetalation step proceeds slowly, with electron transfer confined to directly participating functional groups. These findings provide an important perspective for the rational design of catalytic reactions.

In conclusion, the present ROET analysis suggests that the exceptional efficacy of organoboronic acid derivatives in Suzuki–Miyaura reactions arises from their ability to act as efficient electron transfer channels when coordinated to a metal center, thereby facilitating C–C bond formation.

4. Conclusions

In this study, we theoretically elucidated the electron motion driving the transmetalation process, which is a key step in the Suzuki–Miyaura cross-coupling reaction, using reactive orbital energy theory (ROET) analysis. ROET is an orbital-energy-based electronic theory that enables the identification of the electron motion responsible for driving chemical reactions, grounded in electrostatic force theory. We investigated the transmetalation mechanism of a reaction involving phenylboronic acid and chlorobenzene, catalyzed by a palladium complex bearing 1,2-bis(dimethylphosphino)ethane as the ancillary ligand, leading to the formation of biphenyl. Two proposed mechanisms, the boronate mechanism and the oxo-palladium mechanism, were examined *via* IRC calculations and subsequently analyzed using ROET. IRC results showed that the boronate mechanism proceeds with a lower activation barrier and a simpler pathway, consistent with experimental observations. ROET analysis revealed an intriguing feature: electron transfer from the boronate anion to the chloro group does not directly drive the

reaction. Instead, it plays an indirect role by facilitating subsequent electron motion from the Pd complex to the boronate moiety, leading to bond formation. Once this bond is established, the boronic acid acts as an electron conduit between the two phenyl groups, enabling electron flow through the Pd center. Furthermore, the ancillary ligand was found to be involved only in the early stage of the transmetalation process, serving as a transient electron donor. This finding supports experimental reports that the ancillary ligand primarily participates in the oxidative addition and reductive elimination steps.

As discussed above, ROET analysis successfully elucidates the electron motion that drives the Suzuki–Miyaura reaction in a manner consistent with experimental observations. In particular, it reveals the distinct electronic roles played by organoboronic acids and ancillary ligands during the transmetalation step. This study offers a new perspective on cross-coupling reactions by focusing on electron motion and supports the utility of ROET analysis as a powerful tool for the rational design of catalytic processes.

Author contributions

Conceptualization, Tsuneda; methodology, Takai, Tsutsumi, and Tsuneda; software, Takai; validation, Tsutsumi; investigation, Takai; writing – original draft, Tsuneda; writing – review and editing, all; visualization, Takai; supervision, Taketsugu; project administration, Tsuneda; funding acquisition, Taketsugu.

Conflicts of interest

There are no conflicts to declare.

Data availability

The data supporting this study are provided as part of the SI.

The ORO images at the steps of the boronate and oxo-palladium processes of the Suzuki–Miyaura cross-coupling reaction, including the reactants, TSs, and products, are illustrated with curly arrows deduced from the ORO variations in Fig. S1 and S2. The orbital energy profiles along the normalized IRCs for each reaction step are summarized in Fig. S3 and S4. The Cartesian coordinates of the optimized geometries of the reactants, TSs, and products are compiled in Table S1. The details of the AFIR calculations used to determine the transition states are also summarized in Scheme S1. Additionally, mp4 files with animations illustrating the changes in OROs along the reaction pathways for each process are also included. See DOI: **https://doi.org/10.1039/d5cp01959a**

References

1 K. C. Nicolaou, P. G. Bulger and D. Sarlah, *Angew. Chem., Int. Ed.*, 2005, **44**, 4442.
2 C. C. C. J. Seechurn, M. O. Kitching, T. J. Colacot and V. Snieckus, *Angew. Chem., Int. Ed.*, 2011, **51**, 5062.
3 K. Tamao, K. Sumitani and M. Kumada, *J. Am. Chem. Soc.*, 1972, **94**, 4374.
4 R. J. P. Corriu and J. P. Masse, *J. Chem. Soc., Chem. Commun.*, 1972, **3**, 144a.
5 N. Miyaura, K. Yamada and A. Suzuki, *Tetrahedron Lett.*, 1979, **20**, 3437.
6 A. O. King, N. Okukado and E. Negishi, *J. Chem. Soc., Chem. Commun.*, 1977, **19**, 683.
7 J. K. Stille, *Angew. Chem., Int. Ed. Engl.*, 1986, 25, 508.
8 Y. Hatanaka and T. Hiyama, *J. Org. Chem.*, 1988, **53**, 918.
9 M. Garcia-Melchor, A. A. C. Braga, A. Lledós, G. Ujaque and F. Maseras, *Acc. Chem. Res.*, 2013, **46**, 2626.
10 G. Frenking and N. Fröhlich, *Chem. Rev.*, 2000, **100**, 717.
11 M. P. Mitoraj and A. Michalak, *J. Mol. Modeling*, 2007, **13**, 347.
12 M. Algarra, C. A. Urbina-Blanco, L. Donnelly, C. M. Beavers, A. L. Rheingold, A. S. Goldman, R. A. Widenhoefer and O. Eisenstein, *Organometallics*, 2012, **31**, 6205.
13 J. E. M. N. Klein, G. Knizia, B. Miehlich, J. Köstner and B. Plietker, *Chem. Eur. J.*, 2014, **20**, 7254.
14 X. Chen, K. M. Engle, D.-H. Wang and J.-Q. Yu, *Angew. Chem., Int. Ed.*, 2009, **48**, 5094.
15 R. A. Dalterio, M. García-Melchor, G. P. A. Yap and J. Rosenthal, *Chem. Eur. J.*, 2021, **27**, 6980.
16 M. Iwasaki and Y. Nishihara, in *Lecture Notes in Chemistry*, ed. Y. Nishihara, Springer, Berlin, 2013, vol. 80.
17 A. A. C. Braga, C. F. de Oliveira, G. R. Genoni, J. B. Domingos, P. M. Esteves, J. M. Batista, A. L. Braga, F. R. Ornellas, H. A. Duarte and R. O. Freire, *et al.*, *J. Am. Chem. Soc.*, 2005, **127**, 929.
18 A. A. C. Braga, G. Ujaque and F. Maseras, *Organometallics*, 2006, **25**, 3647.
19 W. Huang, Z. Weng and X. Hong, *Chem. – Eur. J.*, 2008, **14**, 4426.
20 C. Sicre, A. A. C. Braga, F. Maseras and M. M. Cid, *Tetrahedron*, 2008, **64**, 7437.
21 M. A. Ortuño, A. Lledós, F. Maseras and G. Ujaque, *ChemCatChem*, 2014, **6**, 3132.
22 B. P. Carrow and J. F. Hartwig, *J. Am. Chem. Soc.*, 2011, **133**, 2116.
23 T. Tsuneda and R. K. Singh, *J. Comput. Chem.*, 2014, **35**, 1093.
24 T. Tsuneda, J.-W. Song, S. Suzuki and K. Hirao, *J. Chem. Phys.*, 2010, **133**, 174101(1).
25 T. Tsuneda, S. Maeda, Y. Harabuchi and R. K. Singh, *Computation*, 2016, **4**(23), 1.
26 T. Tsuneda and T. Taketsugu, *Commun. Chem.*, 2025, **8**(158), 1.
27 M. Hasebe, T. Tsutsumi, T. Taketsugu and T. Tsuneda, *J. Chem. Theory Comput.*, 2021, **17**, 6901.
28 T. Tsuneda, H. Sumitomo, M. Hasebe, T. Tsutsumi and T. Taketsugu, *J. Comput. Chem.*, 2023, **44**, 93.
29 N. Takai, T. Tsutsumi, K. Saita, T. Taketsugu and T. Tsuneda, *Sci. Rep.*, 2025, **15**, 1.
30 S. Maeda, Y. Harabuchi, M. Takagi, K. Saita, K. Suzuki, T. Ichino, Y. Sumiya, K. Sugiyama and Y. Ono, *J. Comput. Chem.*, 2018, **39**, 233.
31 S. Maeda, Y. Harabuchi, Y. Sumiya, M. Takagi, K. Suzuki, M. Hatanaka, Y. Osada, T. Taketsugu, K. Morokuma and K. Ohno, GRRM23, 2023, **https://afir.sci.hokudai.ac.jp/**.
32 T. Tsuneda and K. Hirao, *WIREs Comput. Mol. Sci.*, 2014, **4**, 375.
33 J.-D. Chai and M. Head-Gordon, *J. Chem. Phys.*, 2008, **128**(084106), 1.
34 M. A. Iron and T. Janes, *J. Phys. Chem. A*, 2019, **123**, 3761.
35 P. J. Hay and W. R. Wadt, *J. Chem. Phys.*, 1985, **82**, 270.
36 T. H. J. Dunning, *J. Chem. Phys.*, 1989, **90**, 1007.
37 M. J. Frisch, G. W. Trucks, H. B. Schlegel, G. E. Scuseria, M. A. Robb, J. R. Cheeseman, G. Scalmani, V. Barone, G. A. Petersson and H. Nakatsuji, *et al.*, *Gaussian 16 Revision C.01*, Gaussian Inc., Wallingford CT, 2016.
38 T. Tsuneda, R. K. Singh and P. K. Chattaraj, *Phys. Chem. Chem. Phys.*, 2018, **20**, 14211.

This journal is © the Owner Societies 2025

Phys. Chem. Chem. Phys., 2025, **27**, 17261–17269 | **17269**